Title:

Rheological characterization of ethylcellulose-based melts for pharmaceutical applications

Authors:

Francesco Baldi[1], Juri Ragnoli[1], Davide Zinesi[1], Fabio Bignotti[1], Francesco Briatico-Vangosa[2], Federica Casati[3], Giulia Loreti[3], Alice Melocchi[3], Lucia Zema[3]*

Affiliations:

[1]Dipartimento di Ingegneria Meccanica e Industriale; Università degli Studi di Brescia; Brescia, Italy

[2]Dipartimento di Chimica, Materiali e Ingegneria Chimica “G. Natta”; Politecnico di Milano; Milano, Italy

[3]Dipartimento di Scienze Farmaceutiche, Sezione di Tecnologia e Legislazione Farmaceutiche "Maria Edvige Sangalli"; Università degli Studi di Milano; Milano, Italy

*Corresponding author: Via G. Colombo 71, I-20133 Milano, Italy;
Telephone: +39-02-503-24654;
e-mail address lucia.zema@unimi.it

Running head:

Rheological characterization of ethylcellulose-based melts

Rheological characterization of ethylcellulose-based melts for pharmaceutical applications

Francesco Baldi[1], Juri Ragnoli[1], Davide Zinesi[1], Fabio Bignotti[1], Francesco Briatico-Vangosa[2], Federica Casati[3], Giulia Loreti[3], Alice Melocchi[3], Lucia Zema[3]*

[1]Dipartimento di Ingegneria Meccanica e Industriale; Università degli Studi di Brescia; Brescia, Italy

[2]Dipartimento di Chimica, Materiali e Ingegneria Chimica “G. Natta”; Politecnico di Milano; Milano, Italy

[3]Dipartimento di Scienze Farmaceutiche, Sezione di Tecnologia e Legislazione Farmaceutiche "Maria Edvige Sangalli"; Università degli Studi di Milano; Milano, Italy

*Corresponding author: Via G. Colombo 71, I-20133 Milano, Italy;
Telephone: +39-02-503-24654;
e-mail address lucia.zema@unimi.it

ABSTRACT

Rheological characterization of ethylcellulose (EC)-based melts intended for the production, *via* micro-injection moulding (μIM), of oral capsular devices for prolonged release was carried out. Neat EC, plasticized EC and plasticized EC containing solid particles of a release modifier (filler volume content in the melt around 30%) were examined by capillary and rotational rheometry tests. Two release modifiers, differing in both chemical nature and particle geometry, were investigated. When studied by capillary rheometry, neat EC appeared at process temperatures as a highly viscous melt with a shear-thinning characteristic that progressively diminished as the apparent shear rate increased. Thus, EC as such could not successfully be processed *via* μIM. Plasticization, which induces changes in the material microstructure, enhanced the shear-thinning characteristic of the melt and reduced considerably its elastic properties. Marked wall slip effects were noticed in the capillary flow of the plasticized EC-based melts, with or without release modifier particles. The presence of these particles brought about an increase in viscosity, clearly highlighted by the dynamic experiments at the rotational rheometer. However, it did not impair the material processability. The thermal and rheological study undertaken would turn out a valid guideline for the development of polymeric materials based on pharma-grade polymers with potential for new pharmaceutical applications of μIM.

Keywords: rheology; micro-injection moulding; ethylcellulose; prolonged release

INTRODUCTION

Well-established techniques used to process thermoplastic polymers, such as extrusion and injection moulding (IM), have gained over the years considerable interest in the pharmaceutical field, as the number of papers recently published in the scientific literature and of drug products already on the market demonstrate [1-3]. In some applications, considering the weight, dimensions, or dimension tolerances of molded parts, the manufacturing process should be regarded as micro-injection moulding (μIM) rather than IM. Several advantages have been highlighted with respect to the use of IM techniques for pharmaceutical production. These are mainly relevant to the improvement of manufacturing (cost-effective and eco-friendly processes, scalability, suitability for continuous manufacturing) and technological/biopharmaceutical aspects (versatility of the product design, patentability, achievement of solid molecular dispersions/solutions of the active ingredient) [4]. Functional containers, namely gastroresistant and pulsatile-release capsular devices, were lately prepared by μIM starting from polymers with peculiar properties, i.e. solubility at pH>5.5 and erosion/dissolution after swelling, respectively [5-7]. For drug delivery purposes it would also be interesting to develop new polymeric materials intended for the manufacturing by μIM of prolonged-release capsular devices able to slowly release their contents over 12-24 h after oral administration.

On the other hand, limitations may arise from processing pharma-grade materials, in consideration of their rheological/thermomechanical behaviour in the melt state and of their thermal or chemical stability. Moreover, issues may be associated with the active ingredient and the product requirements, such as drug dose, release profile, stability and compliance. In this respect, a rational design of new polymers, or of a new generation of traditional ones with improved thermal properties, has recently been attempted (e.g. Soluplus®, Affinisol™) [8]. Therefore, the need for a thorough understanding of the thermal and rheological properties of pharma-grade polymeric melts and of their impact on both processing conditions and physico-mechanical stability of the final products becomes of utmost importance [9].

Based on such premises, the aim of this work was to investigate the rheological behaviour of melts based on ethylcellulose (EC), chosen because it is the most widely employed polymer for the preparation of prolonged drug delivery systems and, moreover, has already been processed in the molten state [10-12]. Both neat and plasticized EC was studied. The plasticizer used was triethyl citrate, the relevant effectiveness as a processing aid for EC-based materials being known from the literature [13]. Besides, as preliminary experiments showed that these materials would fail to yield the pursued release performance, two permeability modifiers (a soluble and a swellable polymer) were added to plasticized EC, based on their ability to create pores in the insoluble capsule wall. The rheological behaviour of these systems, which at processing temperatures consisted of suspensions of solid particles in the plasticized EC melt, was then evaluated. The characterization of the EC-based melts was carried out by both capillary and rotational rheometry. Capillary rheometry was employed to study the processability of the materials in view of their μIM, whereas rotational rheometry experiments were performed to gain a more in-depth understanding of the viscoelastic response.

MATERIALS AND METHODS

Materials

Ethylcellulose, EC (Ethocel™ Std. 100 premium; Dow, United States); triethyl citrate, TEC (Aldrich, Germany); KIR (Kollicoat® IR; BASF, Germany); low-substituted hydroxypropyl cellulose, LHPC (L-HPC NBD 020; Shin-Etsu, Japan).

Methods

The following EC-based materials were prepared:

- plasticized EC (pEC): EC powder was placed in a mortar and the liquid plasticizer, TEC (20% by weight on the dry polymer), was manually added under hard mixing. The kneaded product was left

stand at least 12 h at room temperature (21±5°C, 55±5% RH) before it was ground by means of a blade mill (La moulinette, Moulinex®, SEB, France).

- pEC filled with KIR or LHPC particles (pEC/KIR and pEC/LHPC, respectively): KIR powder (d_{50} = 23μm; d_{90} = 55μm) or LHPC powder (d_{50} = 46μm; d_{90} = 129μm), previously desiccated at 40°C in an oven for 24 hours, were mixed in a mortar with pEC in a 3:7 weight ratio. The mixed powders were then stored into bags under vacuum, and characterized within one or two days.

Thermal characterization

Thermal analysis on EC and pEC powders was performed on a calorimeter DSC1 STAR by Mettler Toledo (Switzerland), using nitrogen as a purge gas (70 ml/min). Indium was used as a calibration standard. Samples of about 10 mg were heated in aluminum crucibles from 30 to 200°C, maintained at this temperature for 1 min, cooled down to 30°C and reheated up to 200°C. Both heating and cooling steps were carried out at 5°C/min.

Capillary rheometry experiments

The tests were performed on a capillary rheometer Rheologic 5000 by Instron CEAST (Italy). In this instrument, the flow rate is imposed by a piston and the extrusion pressure monitored by a melt pressure transducer (data recorded every 0.15 s) placed in the barrel at a distance of 15 mm from the die entry plane**; a schematic of a piston velocity-controlled capillary rheometer is reported in Figure 1a**. Preliminary trials were carried out on EC to find suitable test conditions. Long residence times in the melt state promoted chemical degradation processes accompanied by gas formation. As such processes were thermally activated, the maximum test temperature was set at 180°C. 175°C was selected as the reference test temperature; additional tests were carried out at: 165, 170 and 180°C on EC; 150, 165 and 170°C on pEC; 150 and 160°C on pEC/KIR and pEC/LHPC. EC could not be examined under 165°C due to the high viscosity of the melt. Flat entrance circular dies made from Vanadis 30^{TM} steel were employed. A die with diameter, d, of 2

mm and length to diameter ratio, l/d, of 10 was used with all the materials. Additional dies were employed, at 175°C, for: *i)* the investigation of wall slip effects, on pEC-based systems; *ii)* the determination of die entrance pressure losses, on EC and pEC. More in detail, the additional dies were: with reference to *i)*, a die having d = 1 mm and l/d = 10; with reference to *ii)*, dies having d = 2 mm and l/d = 5 and 20, for EC analysis, and a die having d = 1 mm and l/d = 20, for pEC analysis. A barrel with diameter, D, of 15 mm was employed. The apparent shear rate at the die wall, $\dot{\gamma}_{app,w}$, ranged between 17.8 and 560 s^{-1} (with five different levels of $\dot{\gamma}_{app,w}$ per decade, equally spaced on a logarithmic scale, examined from the lowest to the highest). $\dot{\gamma}_{app,w}$ is related to the imposed flow rate, Q, and the die diameter, d, as follows:

$$\dot{\gamma}_{app,w} = \frac{32 \cdot Q}{\pi \cdot d^3} \quad (1)$$

Shear rates lower than 17.8 s^{-1} were not considered because time to the attainment of the steady-state would have been too long and degradation phenomena could occur. The tests at 175°C with l/d = 10 and d = 1 mm or 2 mm dies were carried out at least three times to check repeatability.

In every test performed, the material, after being loaded into the instrument barrel, was subjected to a pre-heating step over 420 s, under a maximum compacting force of 300 N.

All tests with the 2 mm diameter dies were conducted in such a way that the various melts experienced the same pre-fixed flow-history, in consideration of the possibility that the materials underwent residence time-controlled chemical processes while in the melt state. More in detail, the period of time during which a material was subjected to a specific $\dot{\gamma}_{app,w}$ (step) was fixed. Preliminary tests allowed to set the duration of each step (Δt_{step}), chosen in such a way as to guarantee the reaching of flow conditions which could be considered representative of a steady-state for every material, at the different test conditions (temperatures and, for EC, also die lengths). Δt_{step} varied between 12 and 20 s, at the highest and the lowest $\dot{\gamma}_{app,w}$ explored, respectively. With

l/d fixed, in a 1 mm die test Δt_{step} had to be higher than in a 2 mm die test, at a given $\dot{\gamma}_{app,w}$, due to the lower absolute time scale of the compression process experienced by the melt in the reservoir (with a 1 mm die the fluid is forced to enter into the capillary with a flow rate that is one eighth of the flow rate used with a 2 mm die).

Rotational rheometry experiments

Measurements of the linear viscoelastic properties were carried out using the strain-controlled rheometer ARES G2 by TA Instruments (Unites States). Dynamic frequency sweep experiments under low amplitude (2%) oscillations were carried out with a parallel-plate geometry**; a schematic of a strain-controlled rotational rheometer with parallel-plate geometry, for oscillatory shear measurement, is reported in Figure 1b**. The diameter of the plates was 25 mm, and the gap was set between 1.3 and 1.8 mm. Preliminary experiments, carried out to identify the adequate test conditions, put in evidence that the results were generally dependent on the overall duration of the test (practically determined by the lower limit of the frequency range explored). This should be attributed to chemical degradation processes, the impact of which is expected to increase with the residence time. Thus, the lower limit of the frequency range explored was set at a relatively high value (10 rad/s). Frequency ranged from 10 to 500 rad/s; ten different frequencies, equally spaced on a logarithmic scale (except 500 rad/s), were examined from the lowest to the highest. The tests were performed on EC at four different temperatures, equally spaced between 160 and 175°C, and on the pEC-based systems, at six different temperatures, equally spaced between 150 and 175°C. Each test was carried out three times at each temperature, to check repeatability.

The materials were placed on the rheometer in the form of disks, with diameter of 25 mm, prepared *via* compression moulding on a P200E press by Collin (Germany). During the compression operation, the material was maintained for 280 s under the pressure of 32 bar, at 183°C for EC and 145°C for the pEC-based systems.

Scanning Electron Microscopy, SEM, analyses

SEM analyses were carried out both on KIR and LHPC powders, and on the fracture surfaces of the extrudates of the filled pEC-based materials, obtained with the tests at the capillary rheometer.

With reference to the analyses on the powders, these were carried out on gold coated powders in a scanning electron microscope (model Zeiss Evo 50 EP) operated in high vacuum mode.

With reference to the analyses on the extrudates, for each material examined, a portion of the extruded filament was collected at the exit from the rheometer die during an experiment at 175°C, with the 2 mm die with l/d = 10, at a $\dot{\gamma}_{app,w}$ of 100 s^{-1}. The filament was then broken under liquid nitrogen, in such a way to obtain a fracture surface almost perpendicular to the direction of the flow in the capillary, and the cryo-fractured surface was observed by a scanning electron microscope (model LEO EVO 40). The surface, prior to be analysed, was sputtered with a thin layer of gold.

RESULTS AND DISCUSSION

Thermal response

Figure **2** shows the thermograms of EC and pEC obtained from the first and the second heating scan, respectively. EC exhibits an endothermic peak, close to 190°C, whereas a similar endothermic peak was not observed in pEC heating scans. This endothermic peak, which was observed in both heating scans and thus related to a reversible thermal process, may be ascribed to the melting of high order (crystalline) domains, as suggested by Davidivich-Pinhas et al. [14] with respect to the same EC grade. This would indicate that EC has a semi-crystalline nature that it maintains up to around 190°C. Interestingly, based on the absence of this endothermic peak in the pEC trace, it could be inferred that plasticization with TEC makes the polymer amorphous. The glass transition of EC was clearly detected in the second heating scan only (glass transition temperature, T_g, around 130°C), because the thermal response in the first heating scan was complicated by the very broad peak around 100°C probably relevant to water evaporation. A similar

broad peak was found also in the first heating thermogram of pEC, the glass transition of which could not be identified even in the second heating scan.

Capillary rheometry experiments

Extrudate appearance

Following rheometry tests on the EC melt, defect-free (at a macroscopic scale) extrudates were always obtained, except at the highest $\dot{\gamma}_{app,w}$ explored (that is 560 s^{-1}). At this apparent shear rate, the presence of bubbles of size comparable to the extrudate cross-section was noticed, irrespective of the working temperature. The formation of these bubbles, observed for the melt that stayed longer in the reservoir of the rheometer ($\dot{\gamma}_{app,w}$ of 560 s^{-1} corresponds to the highest residence time in the rheometer), might be explained as the consequence of chemical degradation processes [15]. This was supported by results obtained from infrared spectroscopy analyses (data not reported).

pEC melt showed two distinct flow regimes within the range of $\dot{\gamma}_{app,w}$ explored in the tests carried out between 165 and 175°C: *i)* a stable steady flow regime, at low levels of $\dot{\gamma}_{app,w}$, and *ii)* an unstable flow regime characterized by the occurrence of melt fracture phenomena, at high levels of $\dot{\gamma}_{app,w}$. The transition from the stable to the unstable regime was detected from the extrudate aspect, whereas no effects on the pressure signal trend occurred. The extrudate from the former regime appeared undistorted, appreciably transparent and with a relatively smooth surface. In the unstable regime, a highly deformed and semi-transparent extrudate, characterized by regular wavy distortions with a typical length around 3 mm, was obtained. Interestingly, the level of $\dot{\gamma}_{app,w}$ at the onset of melt fracture decreased by lowering the test temperature, from 560 s^{-1} at 175°C to 178 s^{-1} at 165°C. Extrudates at 150°C were different as compared to those obtained at higher

temperatures (distortions were in general more irregular and less marked) and appeared deformed in the whole range of $\dot{\gamma}_{app,w}$ explored.

With pEC/KIR and pEC/LHPC melts, at the highest $\dot{\gamma}_{app,w}$ explored (that is 560 s^{-1}), large amplitude fluctuations in the pressure signal were recorded and acceptable steady-state extrusion pressure data could not be measured. Fluctuations could not be ascribed to the occurrence of melt fracture phenomena, since no flow instability could be recognized, and the processes at the basis of their origin are not clear. Due to the presence of the KIR and LHPC particles, the extrudate appeared opaque and with a considerably rough surface. Figures **3**a and b show SEM images of these particles. KIR particles have pseudo-spherical shape and smooth surface, whereas LHPC particles appear as flakes or short fibres with rough surface. Figures **3**c and d show higher magnification SEM images of the fracture surfaces obtained from the pEC/KIR and pEC/LHPC extrudate, respectively. It is worth underlining that both KIR and LHPC particles maintained their solid state at the test temperatures. LHPC particles appear better wetted by the polymer with respect to KIR ones. SEM images of the same surfaces at lower magnification (data not reported) showed that both types of particles are uniformly dispersed within the polymeric matrix.

Apparent viscosity functions

Figures **4**a-d show the steady-state apparent shear viscosity, η_{app}, *vs* apparent shear rate at the die wall, $\dot{\gamma}_{app,w}$, curves obtained for EC and the pEC-based melts at different temperatures and with the die having d = 2 mm and l/d = 10. At a given $\dot{\gamma}_{app,w}$, η_{app} is evaluated as the ratio between the apparent shear stress at the die wall, $\tau_{app,w}$, and $\dot{\gamma}_{app,w}$, with $\tau_{app,w}$ calculated from the steady-state extrusion pressure, ΔP, uncorrected for the die entrance pressure drop, ΔP_{ent}, as:

$$\tau_{app,w} = \frac{\Delta P}{4 \cdot l/d} \qquad (2)$$

Data at 175°C are the average of three replicated measures (bars in figure represent the standard deviation; when not visible, they are shorter than the symbol height). Working with EC at 165°C, $\dot{\gamma}_{app,w}$ higher than 178 s^{-1} could not be determined since extrusion pressure exceeded the maximum capacity of the pressure transducer (50 MPa). Data indicated with open or thinner symbols and connected by dotted segments should be regarded as critical since melt fracture occurred (for pEC) or acceptable values of steady-state extrusion pressure could not be detected (for EC and filled pEC-based melts, at $\dot{\gamma}_{app,w}$ = 560 s^{-1}).

The pronounced effect of the test temperature on the viscosity of EC melt is clearly shown in Figure **4**a. Under the assumption that the relationship between ΔP_{ent}, and the true shear stress at the die wall, τ_w, is temperature invariant [16], the time-temperature superposition principle was tentatively applied to the $\tau_{app,w}$ data obtained. Each logarithmic plot of $\tau_{app,w}$ *vs* $\dot{\gamma}_{app,w}$ referred to a specific temperature, T, was horizontally shifted to overlap as much as possible the reference curve at T_0 = 175°C. Such a procedure permitted to evaluate, for each temperature, the shift factor, a_T, at constant $\tau_{app,w}$, averaged over the shear stress range explored. Good results with respect to the overlapping were generally obtained, and the shift factor turned out practically independent from the stress level within the whole shear stress range explored. This appears rather surprising taking into account the complex evolving micro-structure of the EC melt.

An Arrhenius type dependence on temperature was observed for a_T, and a viscous flow activation energy, $E_{0,s}$, of ≈240 kJ/mol was obtained (see [16] for Arrhenius equation) – the subscript "s" is used in $E_{0,s}$ to indicate that the activation energy is derived from steady-state flow properties. By considering that, for an ordinary industrial polymer melt, the viscous flow activation energy derived from fully developed flow tests is of the order of a few tens of kJ/mol and typically keeps smaller than 100 kJ/mol [17,18], the value of $E_{0,s}$ obtained for EC seems very high. The pronounced sensitivity of apparent viscosity to temperature could be related to the thermal response of EC. Due to the tendency to undergo chemical degradation processes at high temperatures, the test

temperatures have been kept relatively low, just below the endothermic peak ascribed to the melting of the crystalline domains (see *Thermal response* section). At the test temperatures, EC melt is expected to have a heterogeneous microstructure with high order regions dispersed within an amorphous matrix and, therefore, it can be argued that small temperature variations can induce substantial changes in the material microstructure and in polymer chains mobility. These temperature-induced microstructural modifications are likely to be reflected in the viscous response obtained in the capillary rheometer, which varied widely with temperature. A contribution of thermally activated chemical processes occurring during the rheometry test, which could reduce the length of the polymeric chains and, therefore, the viscosity of the material, could not be ruled out. It is worth noting that the phenomena described above do not explain the "apparent thermorheological simplicity" observed for EC. A comprehensive analysis of the processes that govern the temperature dependence of the viscosity here observed would require an extensive work aimed at studying the chemical-physical processes undergone by EC during a capillary rheometer test, and it could be a matter of further studies.

From a_T data, the η_{app} *vs* $\dot{\gamma}_{app,w}$ master curve of EC was constructed at $T_0 = 175°C$ (data at 560 s^{-1} have been removed). In Figure **4**a, shifted data-points [($\dot{\gamma}_{app,w} \cdot a_T$; η_{app}/a_T) where a_T is temperature shift factor] are indicated with grey symbols, and dashed line is sketched as a guideline for the eye. The EC melt shows a non-Newtonian behaviour, apparently shear-thinning, but different from that of an ordinary polymer melt. It is characterized by a threshold level of apparent viscosity, $\eta_{app,\infty}$ ($\eta_{app,\infty} \approx 670$ Pa·s), approached at high shear rates. This behaviour recalls that of Bingham fluids [19], even if in this case the existence of a yield stress cannot be firmly stated on the basis of the data obtained. The presence of a threshold at a relatively high level of viscosity clearly indicates that EC can be very hardly processed *via* μIM, at least at process temperatures compatible with its chemical stability. This was confirmed by explorative μIM tests, performed with a μIM press (BabyPlast 6/10P; Cronoplast S.L., Barcelona, Spain) equipped with a disk-shaped screening

mould (the details of machine and mould used are reported in [7]). At process temperatures comparable with those used in the capillary rheometer tests, EC could not be processed if un-plasticized.

For comparison purposes, the flow curve (master curve at T_0 = 175°C) of EC is also reported in Figures **4**b-d relevant to pEC-based melts. From Figure **4**b it can be observed that the plasticization with TEC makes the rheological response of pEC consistent with that of an ordinary polymer melt. The trend of the flow curve does not indicate the existence of a threshold level of apparent viscosity and, at the highest $\dot{\gamma}_{app,w}$ explored, η_{app} of pEC is remarkably lower than that of EC (at 175°C). This suggests for the pEC melt the possibility to be processed *via* μIM. By comparing the flow curves of pEC/KIR and pEC/LHPC, reported in Figures **4**c and d, respectively, with that of pEC, it emerges that the presence of a secondary phase in pEC, either KIR or LHPC particles, promotes an increase in η_{app}, at a given level of $\dot{\gamma}_{app,w}$, without impairing the shear-thinning nature of the response, and therefore the potential for the material to be processed at high shear rates. Also these assumptions were confirmed by preliminary μIM trials performed as above described.

As shown in Figures **4**b-d, the test temperature leaves the apparent viscosity function of pEC-based melts practically unchanged. This seems to suggest that the flow of these materials is not governed by the shear viscosity of the melt, and that a more complex flow takes place. Moreover, for unfilled pEC the test temperature was already shown to influence the level of $\dot{\gamma}_{app,w}$ at the onset of melt fracture phenomena (see *Extrudate appearance* section), which are generally related to a complex equilibrium between adhesion and slip of the polymer melt at the wall metal interface [20,21]. As polymer/wall interface processes can play a role in defining the capillary flow of the pEC-based melts, the occurrence of wall slip effects in the capillary flow of these melts was verified.

Wall slip effects were studied by the application of the Mooney technique [22]. This approach assumes that the fluid is homogeneous and the slip velocity at the die wall, v_s, is a function of the wall shear stress, τ_w, only. The apparent shear rate at the die wall, $\dot{\gamma}_{app,w}$, which the polymer melt is subjected to during capillary flow at a given τ_w, results from: (i.) a purely viscous bulk contribution, $\dot{\gamma}_{app,w,v}$, that would only depend on the intrinsic behaviour of the material, and (ii.) a wall slip contribution, $\dot{\gamma}_{app,w,s}$, that depends on v_s and die diameter, d, according to Eq. 3:

$$\dot{\gamma}_{app,w,s} = \frac{8}{d} \cdot v_s(\tau_w) \quad (3)$$

Tests with different die diameters are carried out and τ_w *vs* $\dot{\gamma}_{app,w}$ curves are obtained. v_s and $\dot{\gamma}_{app,w,v}$ can thus be determined from the slope and the intercept, respectively, of the least square regression straight line that interpolates the $\dot{\gamma}_{app,w}$ *vs* 1/d data (Mooney plot), at a given level of τ_w. In this work, under the assumption that ΔP_{ent}, do not significantly change with the die diameter (supported by the experimental observation that for pEC the levels of ΔP_{ent} measured with the highest contraction ratio, D/d, available are very small, as shown below, in the *Entrance pressure losses* section), extrusion pressure data uncorrected for ΔP_{ent} were used, and $\tau_{app,w}$ rather than τ_w data were employed. By considering that slip phenomena can depend in principle also on the extrusion pressure [23], the dies for wall slip analysis were chosen in such a way that similar levels of steady-state extrusion pressure were reached in the experiments. More specifically, data from tests carried out, at 175°C, with dies having different diameter (d = 1 and 2 mm) but same l/d (l/d = 10) were used. In Figure **5** the $\tau_{app,w}$ *vs* $\dot{\gamma}_{app,w}$ curves obtained with the two different dies for pEC, pEC/KIR and pEC/LHPC are compared (bars in figure represent the standard deviation; when not visible, they are shorter than the symbol height). The data obtained with the 2 mm die at 560 s^{-1} were not taken into account; for pEC, also the datum obtained with the 1 mm die at 560 s^{-1} was

omitted since melt fracture was observed. The curve obtained with the 2 mm die is above the 1 mm die curve over the whole range of $\dot{\gamma}_{app,w}$, independent of the material, thus indicating that slip effects occur. It is worth noting that, contrary to what generally observed for melts based on ordinary polymeric materials exhibiting wall slip in capillary flow [23], at the highest levels of $\tau_{app,w}$ (that is of ΔP) the curves obtained with the different dies tend to get closer. For pEC, they even overlap at the highest $\dot{\gamma}_{app,w}$, indicating that, for this material, high levels of ΔP, close to the onset of melt fracture phenomena, lead to slipping suppression. Considering that (i.) $\dot{\gamma}_{app,w}$ data from the curves obtained with the two different die diameters, at a given $\tau_{app,w}$, refer to different residence times in the rheometer (longer for the 1 mm die), and that (ii.) the linearity of the Mooney plot, corresponding to a given $\tau_{app,w}$, could not be proven since only two diameters were used, only slip velocity was determined and referred to as an "apparent slip velocity" (indicated with $v_{s,app}$). In Figure **6**, $v_{s,app}$ is reported as a function of $\tau_{app,w}$ for pEC and the filled pEC-based systems, in a double-logarithmic plot. For pEC, the downward arrow indicates the tendency of slipping phenomena to be suppressed at high levels of $\tau_{app,w}$. As the dependence of $v_{s,app}$ on $\tau_{app,w}$ within the explored range of $\tau_{app,w}$ appeared of power-law-type (linear in a double-logarithmic plot), as for ordinary polymer melts, with particular reference to polyolefins [23,24], data were accordingly fitted. In Figure **6**, power-law fitting curve (dashed line) is traced for each series of data (for pEC the point at $\tau_{app,w}$ = 76770 Pa, indicated with an open symbol, was not included in the fitting). The order of magnitude of the slip velocity obtained for the pEC-melts is comparable with that of polyolefin-based melts, but the levels of shear stress at which wall slip phenomena occur are generally lower [23,25]. With respect to the unfilled pEC, the presence of a secondary phase, in pEC/KIR and pEC/LHPC, promotes a decrease in $v_{s,app}$, at a given level of $\tau_{app,w}$, but enlarges the $\tau_{app,w}$ range of slip, allowing high values of $v_{s,app}$ to be reached. This latter effect is due to the different sensitivity of $v_{s,app}$ on $\tau_{app,w}$, exhibited by pEC and the filled pEC-based melts, here

represented by the slope of the power-law fitting line (that is 2.0 for pEC, 3.4 and 4.0 for pEC/KIR and pEC/LHPC, respectively). Most of the flow occurs by wall slip, and the slip contribution to the flow rate decreases by increasing the shear stress level; at the lowest level of $\tau_{app,w}$, for the capillary with the highest surface/volume ratio (that is the 1 mm die), it is approximately the 90, 80 and 70% of the imposed flow rate for pEC, pEC/KIR and pEC/LHPC melt, respectively. It can be thought that the pronounced wall slip effects of pEC-based melts are due to the presence of the plasticizer, TEC, which, during the capillary flow, could migrate at the die wall. This hypothesis should be confirmed with specific analyses, which could be a matter of further studies.

Entrance pressure losses

Figures **7**a and b show Bagley plots constructed from the steady-state extrusion pressure, ΔP, data measured at various $\dot{\gamma}_{app,w}$, at 175°C, for EC and pEC, respectively; for EC, ΔP data were measured in tests carried out with dies having diameter of 2 mm (data at 560 s^{-1} were not included in the analysis) whereas, for pEC, in tests with 1 mm dies. At l/d = 10, each datum is the average of three values measured in replicated experiments (standard deviation bars indicated).

In Bagley plot, the experimental (l/d; ΔP) data at a given $\dot{\gamma}_{app,w}$ typically lie on a straight line, and ΔP_{ent} value is determined by extrapolating to zero the least square regression line that interpolates them. From Figure **7**a, it clearly emerges that, for EC, at each level of $\dot{\gamma}_{app,w}$ explored, the dependence of ΔP on the die length to diameter ratio, l/d, is not linear. This curvature of the Bagley plots cannot be related to the effect of pressure on viscosity, nor to slipping phenomena, since these factors would induce an upward shift of curves [23]; it rather might be ascribed, at least for the highest levels of $\dot{\gamma}_{app,w}$, to viscous heating effects, mainly occurring in the longest die (that is the die with l = 40 mm), where they are expected to be more marked [26,27]. In support of this discussion is the observation that EC viscosity is very sensitive to temperature, and a small

383 temperature increase produced by viscous heating can give rise to a pronounced decrease in
384 viscosity (and therefore in ΔP). In accordance with these results, for the determination of ΔP_{ent} of
385 EC, only data obtained with the two shorter dies (with l/d = 5 and 10), and indicated in Figure **7**a
386 wih full symbols, were used.

387 For the pEC melt, too small ΔP_{ent} values were obtained by applying the Bagley procedure to
388 data from tests performed with 2 mm dies. When very small, ΔP_{ent} values can turn out comparable
389 with the statistical error induced by the extrapolation procedure, thus becoming not reliable.
390 Therefore, it is necessary to resort to a test flow geometry that could induce higher level of ΔP_{ent} to
391 be reached. By considering that at a given $\dot{\gamma}_{app,w}$, the higher the reservoir to die diameter ratio,
392 D/d, the higher is ΔP_{ent} (with D fixed) [28], 1 mm dies were used for ΔP_{ent} evaluation, and more
393 reliable ΔP_{ent} data could be obtained except for the lowest $\dot{\gamma}_{app,w}$. In consideration of the fact that
394 pEC shows wall slip phenomena that can be pressure dependent, for the determination of ΔP_{ent} only
395 data obtained with the two shortest dies available (with l/d = 10 and 20) were used (Figure **7**b).

396 For both EC and pEC, at each $\dot{\gamma}_{app,w}$ examined, the value of ΔP_{ent} was determined as the
397 intercept of the straight line traced on the two (l/d; ΔP) valid points (dashed lines in Figures **7**a and
398 b), and, in turn, the true shear stress at the die wall, τ_w, was evaluated. Figure **7** clearly shows that
399 the levels of ΔP_{ent} of EC are considerably higher than those of pEC (for EC, at 316 s^{-1}, ΔP_{ent} is
400 higher than 5 MPa, whereas for pEC, at 560 s^{-1} it does not even reach 1 MPa). In Figure **8**, the ratio
401 between ΔP_{ent} and τ_w is plotted as a function of $\dot{\gamma}_{app,w}$, for both EC and pEC, and power-law fitting
402 curve (dashed line) is traced for each series of data. It clearly emerges that, in the whole range of
403 $\dot{\gamma}_{app,w}$, the level of $\Delta P_{ent}/\tau_w$ obtained for EC is largely higher than that obtained for pEC. By
404 considering that, quoting Jerman and Baird [29], "values of $\Delta P_{ent}/\tau_w$ are thought to represent the
405 elasticity of a polymer melt", this result indicates that plasticization with TEC considerably reduces
406 the elastic character of EC in the melt state. This is further confirmed by the swell behaviour

exhibited by the two extrudates: the diameter of the EC extrudate (evaluated after material solidification on samples obtained from tests carried out at 175°C, with the 2 mm die with l/d = 10) was larger than that of the pEC one. The difference between the two materials increased by increasing the level of $\dot{\gamma}_{app,w}$ undergone by the melt in the capillary flow (at 316 s^{-1}, the diameter of EC extrudate was nearly twice that of pEC). The pronounced elastic character exhibited by the EC melt is probably another reflection, at a macroscopic scale, of its peculiar microstructure.

Rotational rheometry experiments

Figures **9**a and b show the absolute value of the complex viscosity, $|\eta^*|$, and the dynamic storage modulus, G', *vs* frequency, ω, master curves of the various materials, constructed from the data obtained at the various temperatures examined (reference temperature, T_0 = 175°C). Each datum reported in the graphs is the average of three values measured in replicated experiments (bars representing the standard deviation are not reported in the graphs as they were generally shorter than the symbol height). Differently from that observed with the capillary rheometer tests, at the rotational rheometer also for the pEC-based melts a clear effect of temperature was observed. This is probably due to the fact that the shear stress levels reached in these latter tests, remarkably lower than those reached in the capillary experiments, are insufficient to promote slip phenomena. The successful attainment of a master curve for each system examined by shifting the rheological data with respect to frequency, on the basis of the temperature shift factors, a_T, demonstrates the validity of the time-temperature superposition principle [already demonstrated for the EC melt by referring to the capillary rheometer results (see *Capillary rheometry experiments, Apparent viscosity functions* section)]. An Arrhenius type dependence on temperature was observed for a_T, and a flow activation energy, $E_{0,d}$, was obtained for each melt – the subscript "d" is used in $E_{0,d}$ to indicate that this flow activation energy is obtained from flow properties measured in dynamic tests. $E_{0,d}$ values are reported in Table I. For the EC melt, an appreciable difference between the flow activation energy calculated from capillary and rotational rhometer tests was obtained. This difference should

be related to the different mechanical histories experienced by the polymer melt in the two rheometers. $E_{0,d}$ of pEC is largely lower than that of EC. In consideration of the differences between the microstructures of these two melts (see *Thermal response* section), this result seems to support the idea that the high sensitivity to temperature exhibited by EC might be ascribed to the presence of high order domains in its melt microstructure, that were not found in the pEC melt. Finally, the incorporation of either KIR or LHPC particles in the pEC induces an increase in $E_{0,d}$.

From Figure **9** it emerges that the viscoelastic behaviour of the pEC-based melts is that typical of homogeneous polymer melts [30]. With respect to the neat pEC melt, the presence of a secondary phase in pEC/KIR and pEC/LHPC melts induces a significant increase in both G' and $|\eta^*|$, within the explored range of frequency. This result is in agreement with the effects reported in literature for polymer melts filled with rigid particles [19,31], indicating that KIR and LHPC particles enhance the capacity of the pEC melts to store elastic energy and dissipate mechanical energy. Interestingly, LHPC particles appear the most effective in promoting an increase in both dynamic properties. By considering for pEC melt a density of 1.01 g/cm^3 (measured by melt flow rate tests carried out by a Modular Melt Flow Indexer by Ceast-Instron, at 170°C, with an extruding mass of 10 kg, according to ISO 1133-1:2011), and for KIR and LHPC particles density values of 0.94 and 1.29 g/cm^3, respectively (evaluated from volume and mass data collected from three compacts prepared by means of a hydraulic press equipped with flat punches), 32 and 25% of actual filler volume contents in pEC/KIR and pEC/LHPC melts were estimated. This result indicates that the higher effectiveness exhibited by LHPC particles cannot be ascribed to a higher volume content of rigid particles in the melt, but it is intrinsically associated with the nature of these particles, which differ from those of KIR in geometry, surface roughness and chemical composition. Interestingly, by considering that LHPC particles (i.) promote an increase in G' and $|\eta^*|$ that is practically independent of the frequency, and (ii.) leave the out-of-phase angle, δ ($\tan[\delta]=G''/G'$), practically unchanged (data of δ not shown here), with respect to the unfilled melt, the viscoelastic response of pEC/LHPC seems to be governed by the matrix. By contrast, for pEC/KIR melt, the

459 frequency dependence of the dynamic properties and the values of the out-of-phase angle obtained,
460 which are different from those of the matrix, suggest that KIR particles embedded in the polymer
461 melt actively contribute to its viscoelastic response.

462 The viscoelastic behaviour of the EC melt differs considerably from that of the pEC-based
463 melts and this might be ascribed to its particular microstructure. In Figure **10**, the shear viscosity, η,
464 obtained from capillary rheometer tests is compared with the complex viscosity, $|\eta^*|$, obtained from
465 rotational rheometer tests (viscosity data measured at 175°C). η data are determined from data of
466 true shear stress (corrected for ΔP_{ent}), τ_w, and true shear rate (calculated according to the
467 Rabinowitsch–Weissenberg method [30]), $\dot{\gamma}$, both evaluated at the die wall, and are plotted as a
468 function of $\dot{\gamma}$. It emerges that the Cox-Merz rule [30], according to which an approximate
469 agreement exists between $|\eta^*(\omega)|$ and the steady-state shear viscosity, $\eta(\dot{\gamma})$, if the angular
470 frequency, ω in [rad/s], is set equal to the shear rate, $\dot{\gamma}$ in [s^{-1}], is not verified. In fact, within the
471 range of $\dot{\gamma}$ explored, the value of $|\eta^*|$ is roughly 2.5 times that of η. Even by replotting the complex
472 viscosity data as a function of the maximum (or "effective") shear rate experienced in the dynamic
473 tests, that is ω multiplied by the amplitude of the oscillation (0.02 in these experiments), as
474 proposed for filled melts by Doraiswamy et al. [32], steady-state and complex viscosity data do not
475 overlap. The mechanical history experienced by the melt in the two types of rheometer is different
476 with respect to: (i.) the type of flow (a steady-state pressure-induced shear flow in the capillary
477 rheometer, and a dynamic drag-induced shear flow under low amplitude oscillation in the rotational
478 rheometer); (ii.) the residence time (a capillary rheometer test is roughly two times longer than a
479 rotational rheometer test). In addition, the material tested at the rotational rheometer underwent a
480 compression moulding operation prior to be tested. These differences are likely to be at the basis of
481 the differences between viscosity and flow activation energy data obtained with the two types of
482 test. More specifically, with reference to the viscosity, it is reasonable to think that data coming
483 from the capillary rheometer refer to a melt characterized by a higher degree of microstructural

orientation. In spite of the difference between the values of η and $|\eta^*|$, the dependence on the time-variable (either $\dot{\gamma}$ or ω) observed for the two different sets of viscosity data is similar, and may suggest that the shear-thinning characteristic of the melt is being progressively reduced as $\dot{\gamma}$ (or ω) increases. Interestingly, the trend of the viscosity function obtained from the rotational rheometer tests does not suggest the existence of a threshold viscosity for EC melt. This result seems to indicate that the threshold noted for the apparent viscosity ($\eta_{app,\infty}$ in Figure **4**a), coming from capillary rheometer tests, originates in part from the high levels of die entrance pressure losses that this melt exhibits at high $\dot{\gamma}_{app,w}$ (it is worth recalling that η_{app} data were evaluated from data of apparent shear stress, $\tau_{app,w}$, uncorrected for ΔP_{ent}).

CONCLUSION

In this work, a rheological characterization of ethylcellulose (EC)-based melts intended to be used for the production *via* μIM of prolonged-release capsular devices was carried out. Neat EC, EC plasticized with TEC (pEC), and pEC containing particles of either a water soluble polymer (KIR) or a hydrophilic swellable polymer (LHPC), added to enhance the permeability of the EC-based materials in view of their final use, were examined by both capillary and rotational rheometry tests.

Capillary rheometry tests showed that this peculiar melt, which is expected to have a heterogeneous microstructure with high order regions dispersed within an amorphous matrix, exhibits a non-Newtonian, apparently shear-thinning behaviour characterized by a threshold in the steady-state apparent shear viscosity, η_{app}, approached at high flow rates. The existence of this η_{app} threshold indicates that neat EC cannot be practically processed *via* μIM. From both capillary and rotational rheometry experiments EC melt shows a very high sensitivity of viscosity to temperature.

Capillary rheometry tests suggest that plasticization with TEC makes EC (pEC) processable *via* μIM. For the pEC melt, which has a homogeneous amorphous structure, the threshold in the η_{app}

was not observed, and a η_{app} function consistent with that of an ordinary polymer melt was obtained. Plasticization with TEC considerably reduces the elastic character of EC, and fosters the occurrence of pronounced wall slip phenomena in the capillary flow. Also for the pEC melts filled with the permeability modifiers, either KIR or LHPC particles (filler volume content around 30%), most of the capillary flow occurs by wall slip. The presence of these particles in the pEC melt induces an increase in η_{app}, which however does not compromise the material shear-thinning behaviour, and therefore its processability. Rotational rheometry experiments clearly indicate that, in the frequency range explored, both LHPC and KIR particles induce an increase in both the complex viscosity, $|\eta^*|$, and the dynamic storage modulus, G', with LHPC particles being the most effective at promoting this increase. KIR particles seem to actively contribute to the frequency dependency of the dynamic properties, whereas the frequency response of the pEC melt filled with LHPC particles seems to be governed by the matrix.

The study performed on EC turned out to be a valuable guideline for the development of polymeric materials with potential for new pharmaceutical applications of μIM.

ACKNOWLEDGEMENTS

The authors are grateful to: ITW Test and Measurement Italia S.r.l. – Instron CEAST Division (Pianezza, Torino, Italy) for the capillary rheometer kindly placed at authors' disposal; Ms. I. Peroni and Ms. G. Spagnoli of Dipartimento di Ingegneria Meccanica e Industriale of Università degli Studi di Brescia (Italy) for the contribution to the preparation of the materials and for the DSC analyses kindly performed; Ms. V. Ferrari of Dipartimento di Ingegneria Meccanica e Industriale of Università degli Studi di Brescia (Italy) for the SEM analyses kindly performed.

REFERENCES

[1] Lang B, McGinity JW, Williams III RO. Hot-melt extrusion – basic principles and pharmaceutical applications. Drug Dev Ind Pharm. 2014;40:1133-1155.

[2] Repka MA, Shah S, Lu J, Maddineni S, Morott J, Patwardhan K, Mohammed NN. Melt extrusion: process to product. Expert Opin Drug Deliv. 2012;9:105-125.

[3] Zema L, Loreti G, Melocchi A, Maroni A, Gazzaniga A. Injection molding and its application to drug delivery. J Control Release. 2012;159:324-331.

[4] Shah S, Maddineni S, Lu J, Repka MA. Melt extrusion with poorly soluble drugs. Int J Pharm. 2013;453:233-252.

[5] Zema L, Loreti G, Melocchi A, Maroni A, Palugan L, Gazzaniga A. Gastroresistant capsular device prepared by injection molding. Int J Pharm. 2013;440:264-272.

[6] Gazzaniga A, Cerea M, Cozzi A, Foppoli A, Maroni A, Zema L. A novel injection-molded capsular device for oral pulsatile delivery based on swellable/erodible polymers. AAPS Pharm Sci Tech. 2011;12:295-303.

[7] Claeys B, De Coen R, De Geest BG, De la Rosa VR, Hoogenboom R, Carleer R, Adriaensens P, Remon JP, Vervaet C. Structural modifications of polymethacrylates: Impact on thermal behavior and release characteristics of glassy solid solutions. Eur J Pharm Biopharm. 2013;85:1206-1214.

[8] Aho J, Boetker JP, Baldursdottir S, Rantanen J. Rheology as a tool for evaluation of melt processability of innovative dosage forms. Int J Pharm. 2015;494:623-642.

559

560 [9] Zema L, Loreti G, Macchi E, Foppoli A, Maroni A, Gazzaniga A. Injection-molded capsular
561 device for oral pulsatile release: development of a novel mold. J Pharm Sci. 2013;102:489-499.
562

563 [10] Quinten T, Gonnissenn Y, Adriaens E, De Beer T, Cnudde V, Masschaele B, Van Hoorebeke
564 L, Siepmann J, Remon JP, Vervaet C. Development of injection moulded matrix tablets based on
565 mixtures of ethylcellulose and lowsubstituted hydroxypropylcellulose. Eur J Pharm Sci.
566 2009;37:207-216.
567

568 [11] Quinten T, De Beer T, Almeida A, Vlassenbroeck J, Van Hoorebeke L, Remon JP, Vervaet C.
569 Development and evaluation of injection-molded sustained-release tablets containing ethylcellulose
570 and polyethylene oxide. Drug Dev Ind Pharm. 2011;37:149-159.
571

572 [12] Bar-Shalom D, Slot L, Wang Lee W, Wilson CG. Development of the Egalet® technology. In:
573 Rathbone MJ, Hadgraft J, Roberts MS, editors. Modified-release drug delivery technology. New
574 York: Marcel Dekker; 2003.
575

576 [13] Maru SM, De Matas M, Kelly A, Paradkar A. Characterization of thermal and rheological
577 properties of zidovidine, lamivudine and plasticizer blends with ethyl cellulose to assess their
578 suitability for hot melt extrusion. Eur J Pharm Sci. 2011;44:471-478.
579

580 [14] Davidivich-Pinhas M, Barbut S, Marangoni AG. Physical structure and thermal behaviour of
581 ehtylcellulose. Cellulose. 2014;21:3243-3255.
582

583 [15] Lai HL, Pitt K, Craig DQM. Characterization of the thermal properties of ethylcellulose using
584 differential scanning and quasi-isothermal calorimetric approaches. Int J Pharm. 2010;386:178-184.

[16] Laun HM, Schuch H. Transient elongational viscosities and drawability of polymer melts. J Rheol. 1989;33:119-175.

[17] Laun HM. Orientation effects and rheology of short glass fiber-reinforced thermoplastics. Colloid Polym Sci. 1984;262:257-269.

[18] Baldi F, Franceschini A, Bignotti F, Tieghi G, Riccò T. Rheological behaviour of nano-composites based on polyamide 6 under shear and elongational flow at high strain rates. Rheol Acta. 2009;48:73-88.

[19] Larson RG. The Structure and Rheology of Complex Fluids. New York: Oxford University Press; 1999.

[20] Hatzikiriakos SG, Dealy JM. Role of slip and fracture in the oscillating flow of HDPE in a capillary. J Rheol. 1992;36:845-884.

[21] Piau J-M, El Kissi N, Toussaint F, Mezghani A. Distortions of polymer melt extrudates and their elimination using slippery surfaces. Rheol Acta. 1995;34:40-57.

[22] Mooney M. Explicit formulas for slip and fluidity. J Rheol. 1931;2:210-222.

[23] Hatzikiriakos SG, Dealy JM. Wall slip of molten high density polyethylenes. II. Capillary rheometer studies. J Rheol. 1992;36:703-741.

611 [24] Laun HM. Capillary rheometry for polymer melts revised. Rheol Acta. 2004;43:509-528.
612
613 [25] Haworth B, Khan SW. Wall slip phenomena in talc-filled polypropylene compounds. J Mater
614 Sci. 2005;40:3325-3337.
615
616 [26] Cox HW, Macosko CW. Viscous dissipation in die flows. AIChE J. 1974;20:785-795.
617
618 [27] Rosenbaum EE, Hatzikiriakos SG. Wall slip in the capillary flow of molten polymers subject
619 to viscous heating. AIChE J. 1997;43:598-608.
620
621 [28] Baldi F, Ragnoli J, Briatico-Vangosa F. Measurement of the high rate flow properties of filled
622 HDPE melts by capillary rheometer: Effects of the test geometry. Polym Test. 2014;37:201-209.
623
624 [29] Jerman RE, Baird DG. Rheological properties of Copolyester Liquid Crystalline Melts. I.
625 Capollary Rheometer. J Rheol. 1981;25:275-292.
626
627 [30] Macosko CW. Rheology: principles, measurements and applications. New York: Wiley-VCH
628 Inc.; 1994.
629
630 [31] Khan SA, Prud'Homme RK. Melt rheology of filled thermoplastics. Rev Chem Eng.
631 1987;4:205-270.
632
633 [32] Doraiswamy D, Mujumdar AN, Tsao I, Beris AN, Danforth SC, Metzner AB. The Cox-Mertz
634 rule extended: A rheological model for concentrated suspensions and other materials with a yeld
635 stress. J Rheol. 1991;35:647-685.
636

Dear Editor,

we would like to thank the Reviewers for appreciating our work and providing helpful comments.

Please find below an outline explaining how such comments have been addressed.

Reviewer #1

The current manuscript is a lucid read and clearly explains each phenomenon observed while using rotational and capillary rheometry experiments and extending the results and confirming the same to understand the processability of the polymers during thermal extrusion. I recommend to accept the manuscript in its current form.

We kindly thank the reviewer for his comments.

Reviewer #2

Authors are reporting a study of rheological characterization of molten polymer systems using capillary and rotational rheometers. It would be helpful for an average reader if authors could add a schematic figure comparing the measurement principle and sample placement with these two methods.

We followed the suggestion of the reviewer by introducing a new Figure 1 in the manuscript showing the measurement principle and sample placement in both capillary and rotational rheometers. The main text of the manuscript has been changed accordingly (in the revised manuscript Figure 1 has been mentioned at lines 110 and 149, and all the other figures have been renumbered).

Table I

Table I – Flow activation energies, $E_{0,d}$, of melts from dynamic tests at the rotational rheometer.

Material	**$E_{0,d}$ [kJ/mol]**
EC	335
pEC	120
pEC/KIR	140
pEC/LHPC	150

Figure captions

Figure 1 – Schematic of (a) a capillary rheometer (piston velocity-controlled) and (b) a rotational rheometer with parallel-plate geometry (strain-controlled, for oscillatory shear measurement). With reference to (a): v_p, piston velocity; P, resulting pressure in the reservoir. With reference to (b): θ, angular displacement; ω, oscillation frequency; M, resulting torque.

Figure **2** – DSC traces of EC and pEC obtained from the first and the second heating scans (thermograms vertically shifted for clarity).

Figure **3** – SEM images of (a) KIR and (b) LHPC particles, and of cryo-fracture surfaces obtained from the extrudates of (c) pEC/KIR and (d) pEC/LHPC.

Figure **4** – Steady-state apparent shear viscosity, η_{app}, *vs* apparent shear rate at die wall, $\dot{\gamma}_{app,w}$, for (a) EC, (b) pEC, (c) pEC/KIR, (d) pEC/LHPC, from capillary rheometry tests at: 180°C, *circle* (a); 175°C, *square* (a-d); 170°C, *triangle* (a,b); 165°C, *rhomb* (a,b); 160°C, *"×"* (c,d); 150°C, *asterisk* (b-d).

Figure **5** – Apparent shear stress at the die wall, $\tau_{app,w}$, as a function of the apparent shear rate at the die wall, $\dot{\gamma}_{app,w}$, for pEC (*square*), pEC/KIR (*circle*), pEC/LHPC (*triangle*), from capillary rheometry tests at 175°C, with d = 2 mm (full symbols) and d = 1 mm (open symbols).

Figure **6** – "Apparent wall slip velocity", $v_{s,app}$, as a function of the apparent shear stress at the die wall, $\tau_{app,w}$, for pEC (*square*), pEC/KIR (*circle*), pEC/LHPC (*triangle*), from capillary rheometry tests at 175°C.

Figure **7** – Bagley plots for (a) EC and (b) pEC, from capillary rheometry tests carried out with dies having d = 2 mm for EC (a) and d = 1 mm for pEC (b), at 175°C. For EC (a), data-points at l/d = 20 (open symbols) not used for ΔP_{ent} determination.

Figure **8** – Ratio between the die entrance pressure drops, ΔP_{ent}, and the true shear stress at the die wall, τ_w, as a function of the apparent shear rate at the die wall, $\dot{\gamma}_{app,w}$, for EC (*rhomb*) and pEC (*square*), from capillary rheometry tests at 175°C.

Figure **9** – (a) Absolute value of the complex viscosity, $|\eta^*|$, and (b) dynamic storage modulus, G', *vs* frequency, ω, master curves (T_0 = 175°C) of EC (*rhomb*), pEC (*square*), pEC/KIR (*circle*) and pEC/LHPC (*triangle*), from rotational rheometry experiments.

Figure **10** – Steady-state shear viscosity, η, *vs* shear rate (at the die wall), $\dot{\gamma}$, curve from capillary rheometry tests (open symbols) compared with the absolute value of the complex viscosity, $|\eta^*|$, *vs* frequency, ω, master curve from rotational rheometry tests (full symbols) for EC, at 175°C.

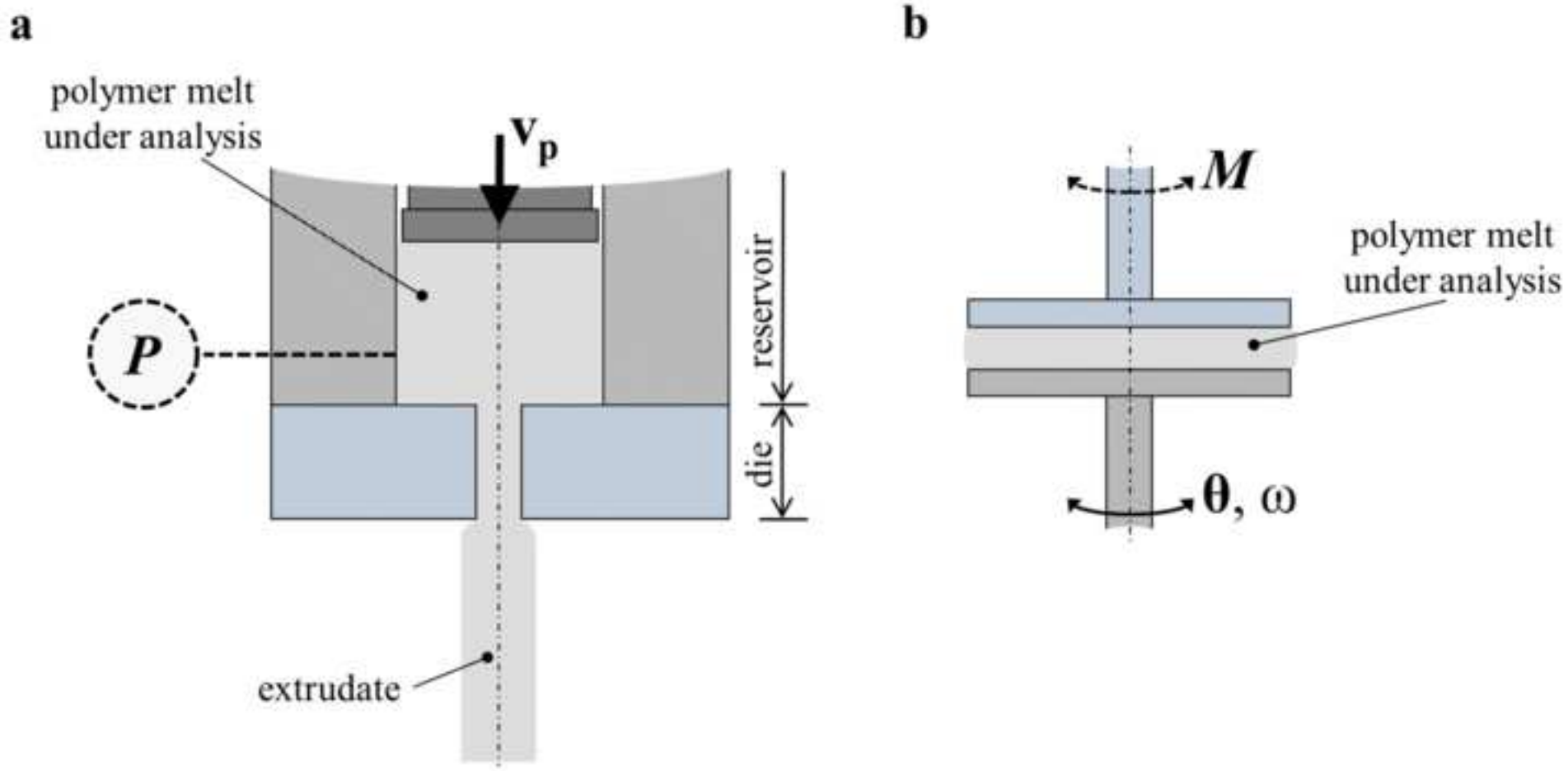

Figure 2

Click here to download Figure Fig 2 revised.tif

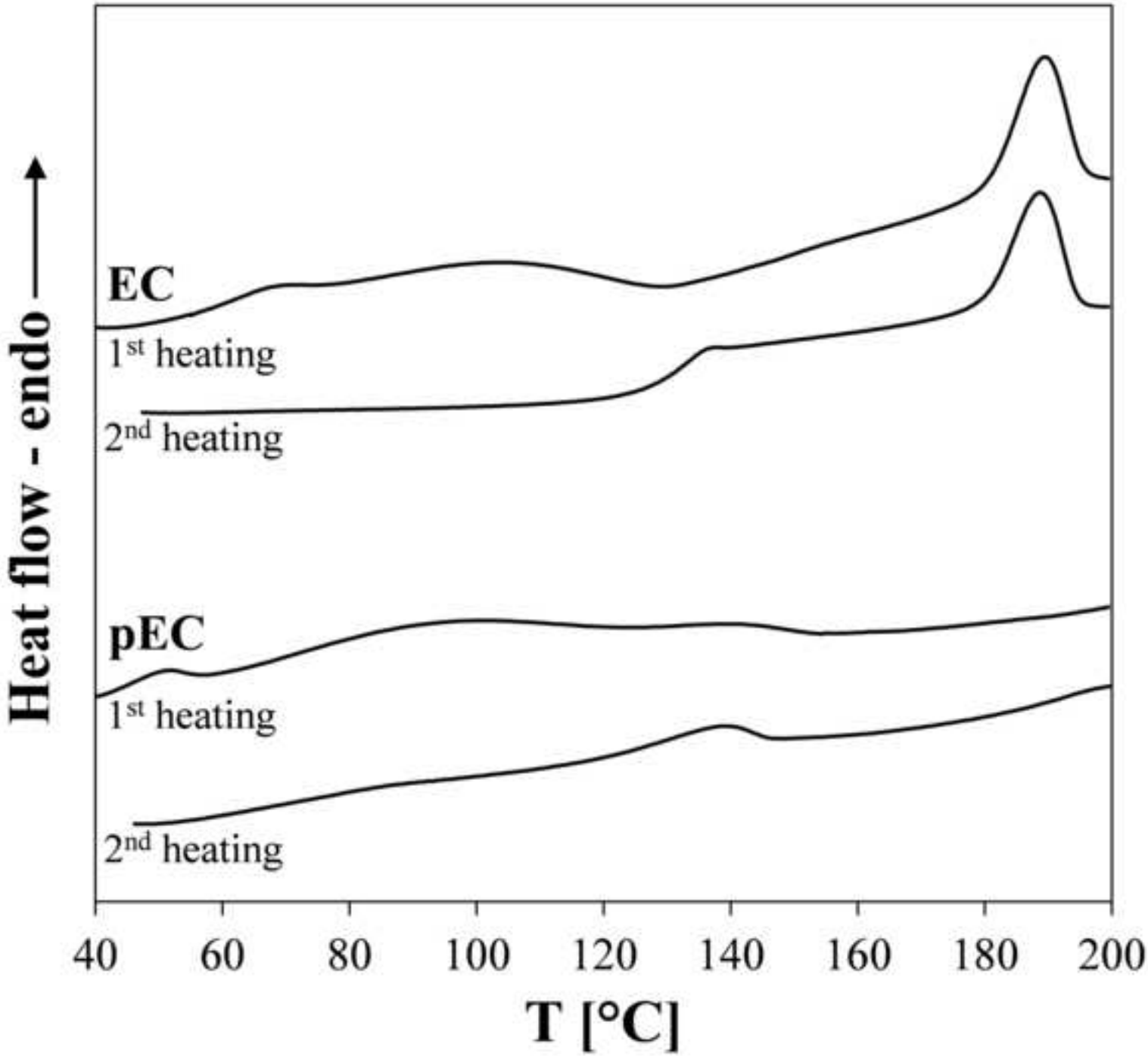

Figure 3

Click here to download Figure Fig 3 revised.tif

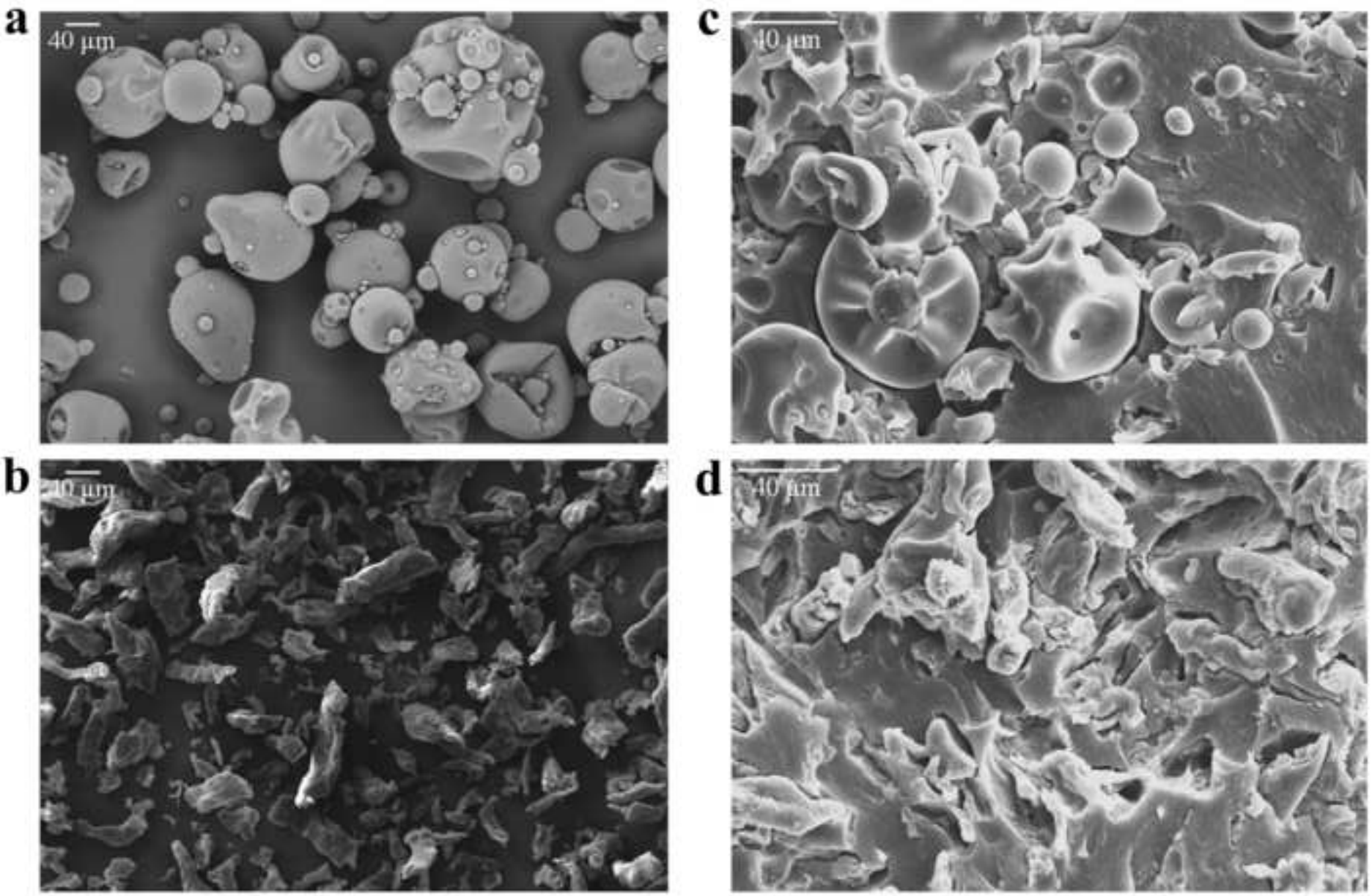

Figure 4

Click here to download Figure Fig 4 revised.tif

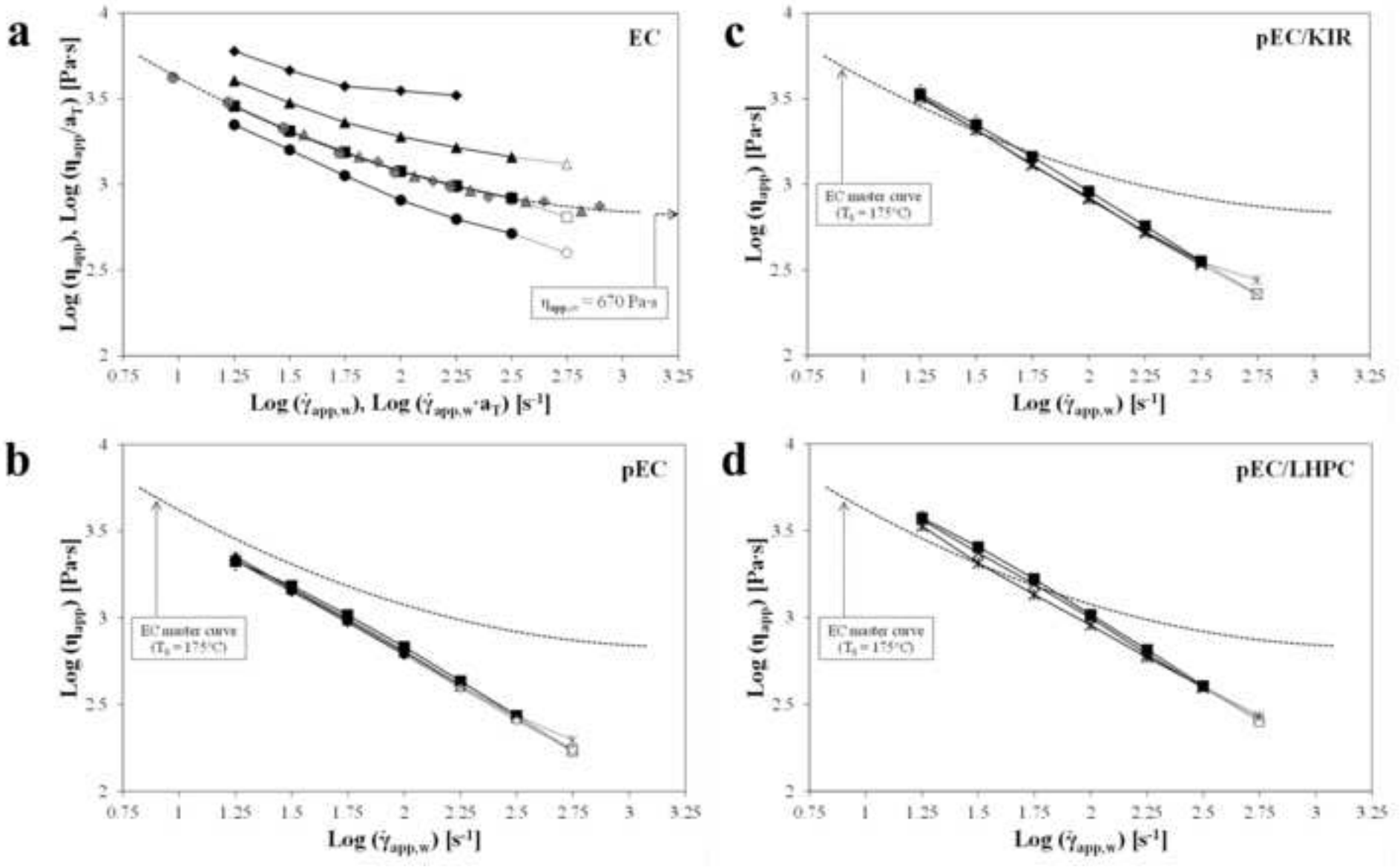

Figure 5

Click here to download Figure Fig 5 revised.tif

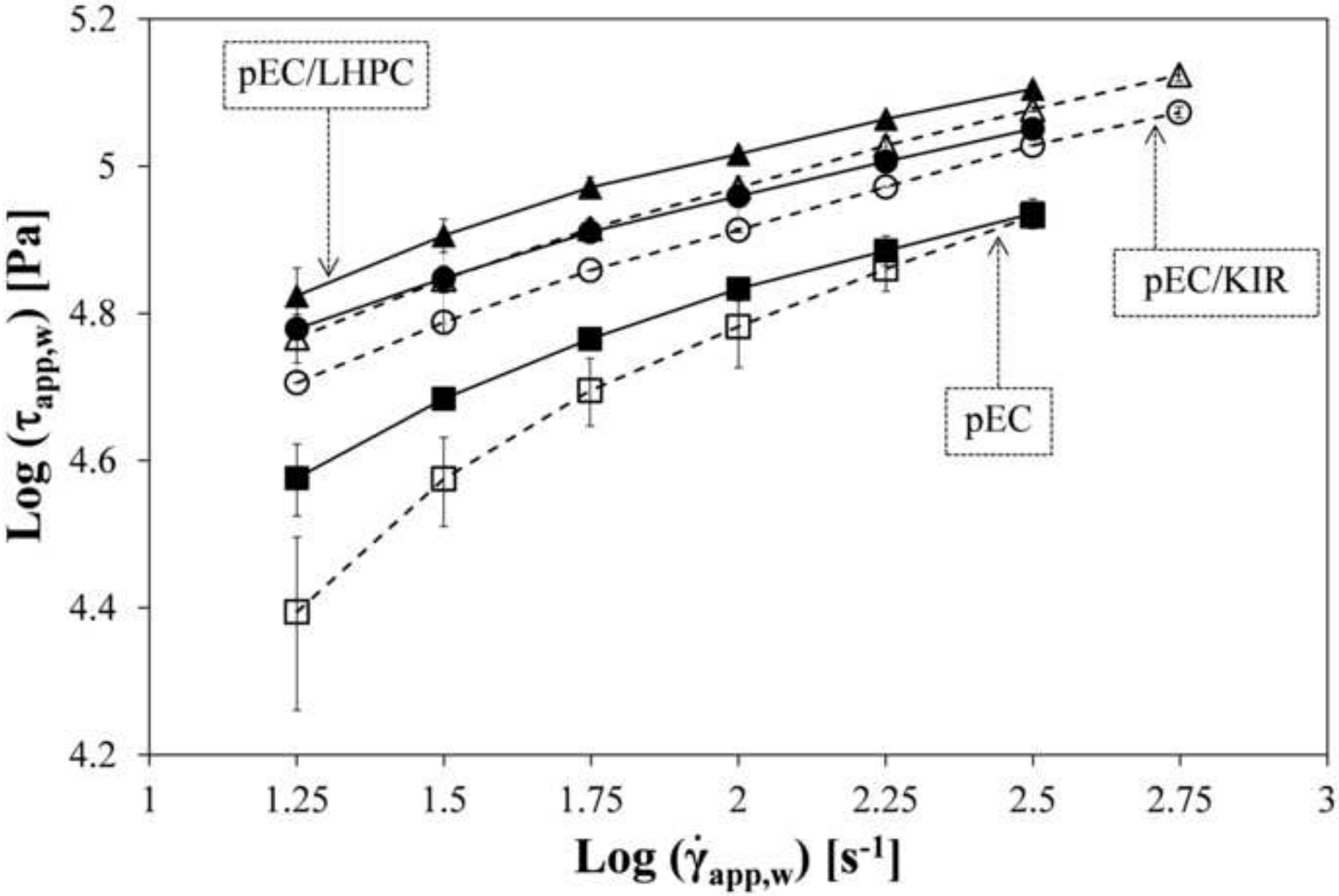

Figure 6

Click here to download Figure Fig 6 revised.tif

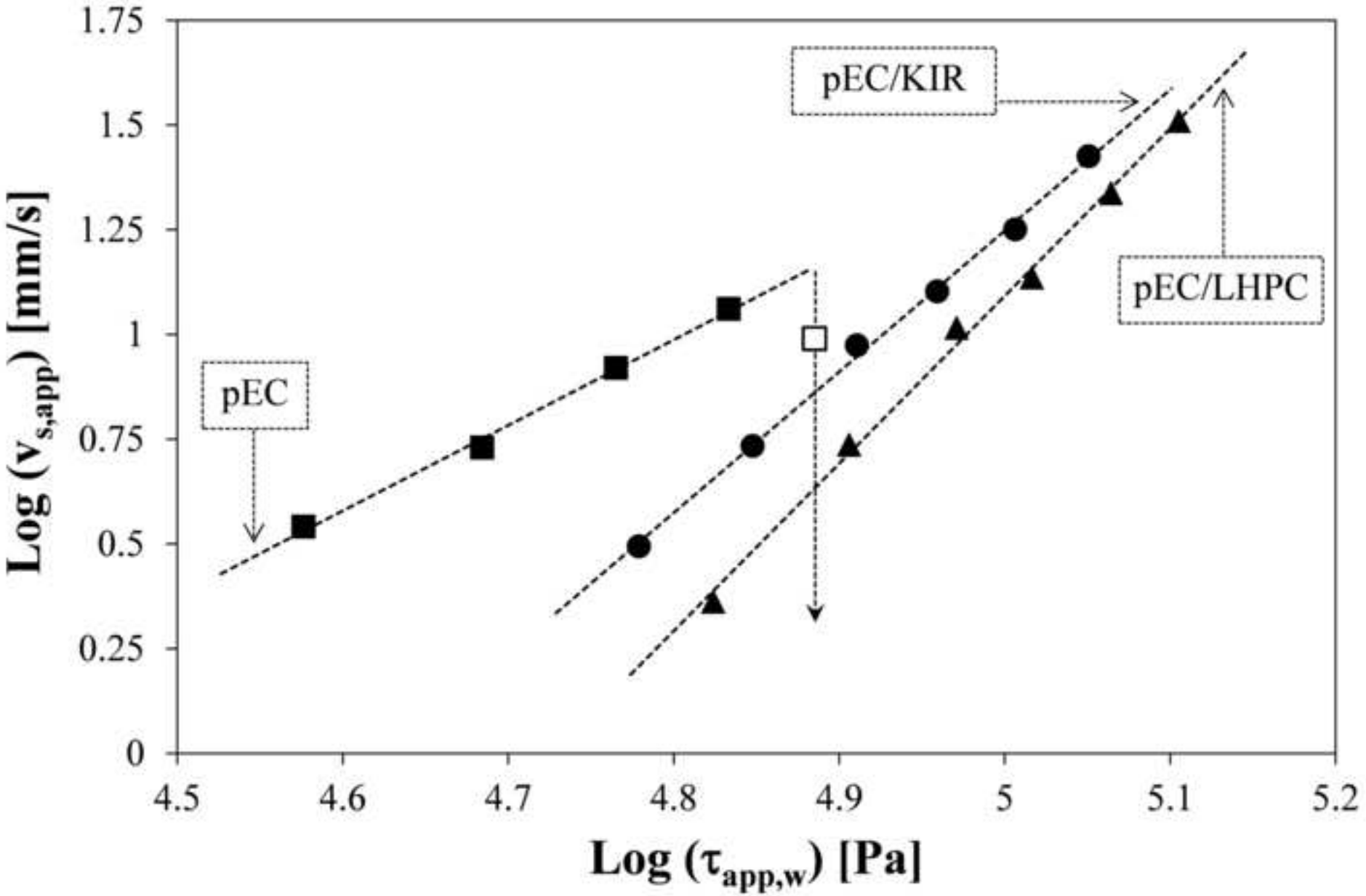

Figure 7

Click here to download Figure Fig 7 revised.tif

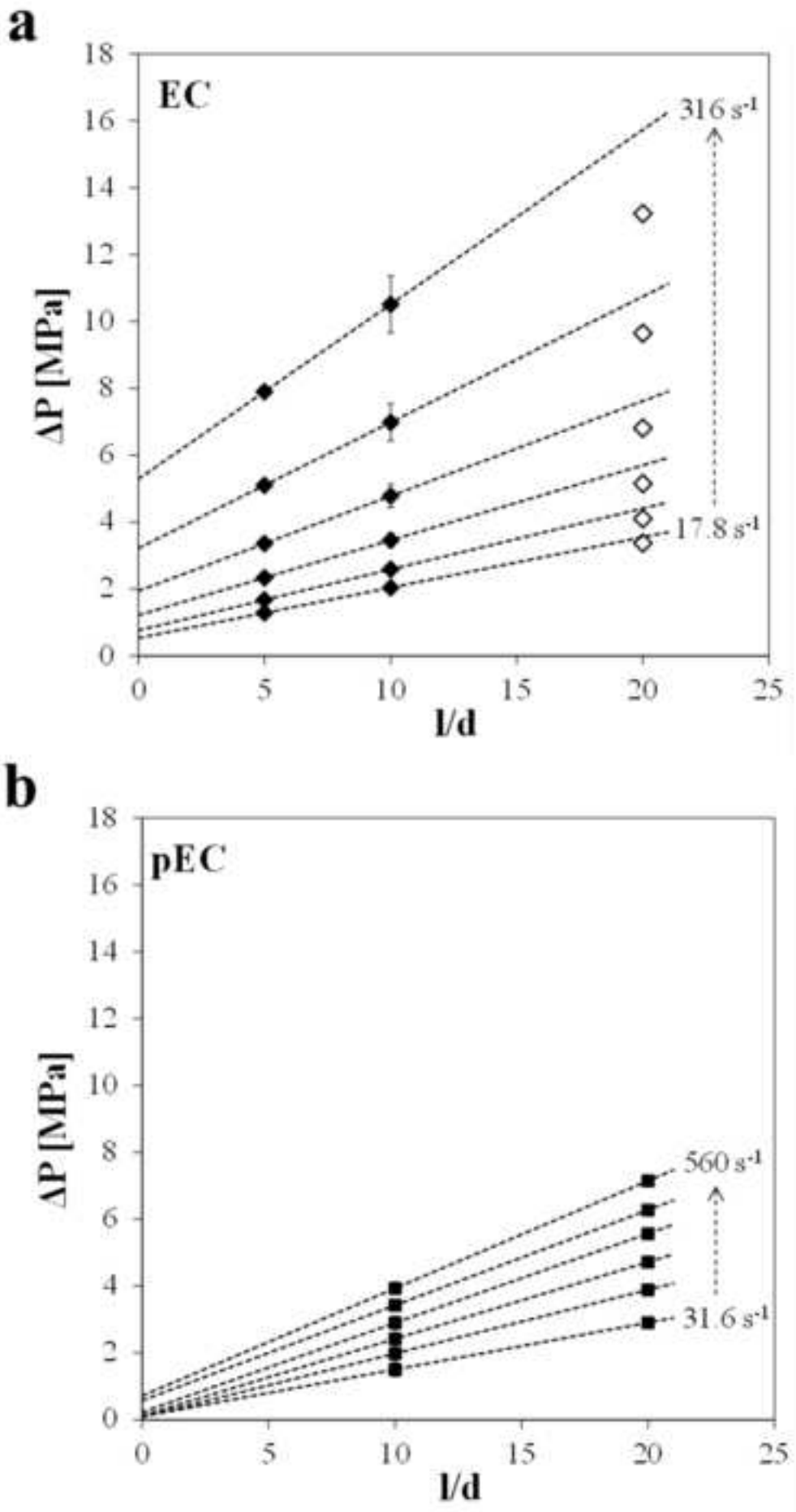

Figure 8

Click here to download Figure Fig 8 revised.tif

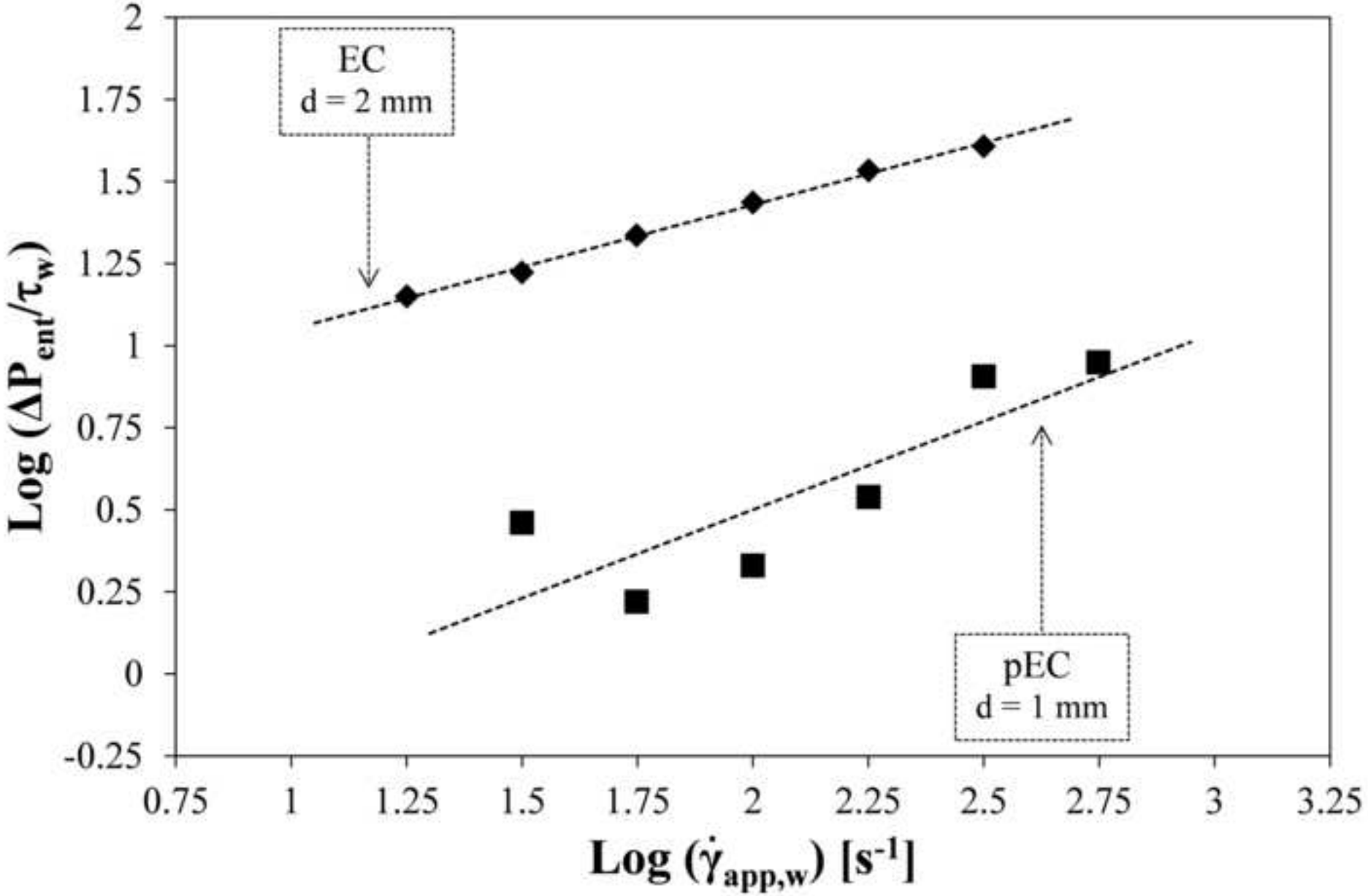

Figure 9

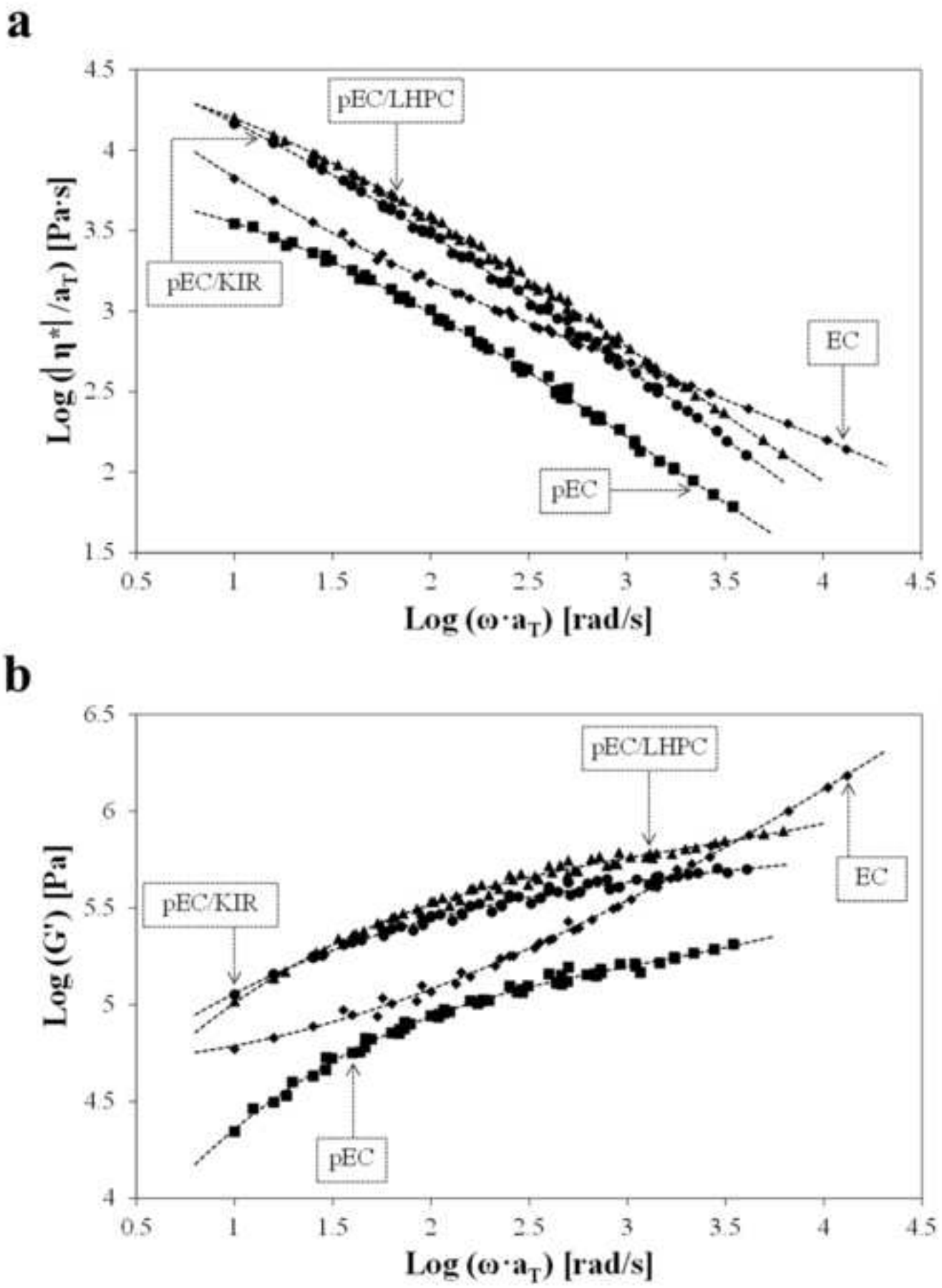

Figure 10

Click here to download Figure Fig 10 revised.tif